TUTORIAL REVIEW

CSR
www.rsc.org/csr

Polarimetric imaging of crystals

Werner Kaminsky, Kacey Claborn and Bart Kahr
Department of Chemistry, Box 351700, University of Washington, Seattle, Washington, USA 98195-1700

Received 5th February 2002
First published as an Advance Article on the web 28th September 2004

Classical crystal optics has recently undergone a renaissance as developments in optical microscopy and polarimetry, enabled in part by sensitive imaging CCD cameras and personal computers, now permit the analytical separation of various optical effects that are otherwise convolved in polarized light micrographs. In this *tutorial review*, we review recent developments in the measurement of the principal crystallo-optical quantities including linear birefringence, linear dichroism, circular birefringence, and circular dichroism, as well as new effects in crystal optics encountered in unusual mixed crystals. The new microscopies and polarimetries are applied to problems of crystallographic twinning, phase transformations, stress birefringence, symmetry reduction, and the design of new crystalline materials.

1. Introduction

Classical crystal optics is the science that involves the simultaneous reckoning of four phenomena, linear birefringence (LB), linear dichroism (LD), circular birefringence (CB), and circular dichroism (CD).[1] These are, respectively, the anisotropy in refraction, the anisotropy in absorption, the difference in the refractive index of left and right circularly polarized light, and the difference in absorption of left and right circularly polarized light. Generally speaking, when more than one of these effects are present at the same time, they are convolved in the elliptical polarization state of the light propagating through the medium. Consequently, complex materials between polarizing elements often present a dazzling array of interference colors whose value is mainly decorative. Polarized light micrographs frequently win scientific art

Werner Kaminsky was born in Cologne, Germany in 1959. He was educated at the Institut für Kristallographie at the university in that city, receiving his diploma, his PhD in crystal physics under the supervision of Siegfried Haussühl, and ultimately his habilitation in 2000. Between 1994 and 1999 he spent several periods as postdoctoral associate, tutor, and lecturer at Oxford University working with A. Michael Glazer on the development of new methods for the analysis of the optical properties of crystals. For this work he received the Philips physical crystallography prize from the British Association of Crystallography. In 2000 he joined the faculty of the Department of Chemistry at the University of Washington, Seattle where he is currently Research Associate Professor.

Kacey Claborn was born in Lindsay, California in 1974. She received her BS in crystallography at the University of Washington in 2001 and expects to complete her PhD at the same institution in 2005. Her research with Bart Kahr and Werner Kaminsky is focused on measurements of the chiroptical properties of crystalline materials. She is the recipient of a graduate fellowship from the organic chemistry division of the American Chemical Society.

Bart Kahr was born in New York City in 1961. He attended Middlebury College in Vermont where he was introduced to research in chemistry by I. David Reingold. His graduate studies of the stereochemistry of unusual molecules with Kurt Mislow at Princeton University were followed in 1988 by postdoctoral research in crystal chemistry at Yale University in the laboratory of J. Michael McBride. In 1990 he joined the faculty of Purdue University and was named a US National Science Foundation Young Investigator. He moved to the University of Washington, Seattle, in 1997 where he is currently Professor of Chemistry. His research group studies the growth, structure, and physical properties of crystalline materials, as well as the history of crystallography.

Werner Kaminsky

Kacey Claborn

Bart Kahr

DOI: 10.1039/b201314m

contests and grace the covers of chemical company catalogs but often mask the underlying nature of the illuminated material.

The analysis of crystals with visible light was a highly developed art prior to the discovery of X-ray diffraction in 1912. At that time, crystallographers shifted their attention in large measure to the determination of the positions of atoms in crystals. Today, X-ray crystallography is a highly developed art. Even the analyses of many biopolymers have been reduced to routine practice. Concurrently, developments in polarimetry, polarized light microscopy, and the advent of CCD cameras coupled to micro-computers have signaled a renaissance in the unfinished science of crystal optics. Only within the past 20 years have the tools been developed for separating the various optical effects from one another thereby maximizing the information about crystal structure and growth that is in principle contained in visible light micrographs. Here, we review these developments with illustrations from our recent work. We have focused these illustrations on a small number of substances – alkali sulfates, sodium halates, and 1,8-dihydroxyanthraquinone – so as to draw various methodologies together in visits to recurrent materials.

2. Differential polarization imaging

The work described herein has so many antecedents as to require a review of nearly two centuries of scholarly work devoted to polarimetry and optical crystallography. Some of this is contained within several review articles[2,40,44] but will not be addressed here in order to ground this work in recent history. The development of differential polarization imaging by Maestre, Tinoco, Bustamante and coworkers in the 1980s serves as an adequate introduction to the tools that we will introduce in the next section. As a foil, coming just before the advent of CCD detectors, it sets off the work that succeeded it. All of the new methods that we have put to use in the study of crystals involve the analysis of intensity signals as a function of the modulation of input polarization. Applications of such a strategy in conjunction with microscopy to form images of LD and CD (or related quantities) can be credited to the aforementioned group.

The relevant body of research was begun in 1985 when Mickols *et al.* introduced the imaging differential polarization microscope.[3] In this device various voltages were applied to a KH_2PO_4 crystal in a Pockels cell in order to modulate between orthogonal polarization states, or between left and right circular polarization states at a frequency of less than 1 kHz. The input polarization was then passed through the sample on a microscope stage. The transmission was analyzed by a linear 256 diode array detector that was translated to produce a 2D image. The difference between the orthogonal polarization states, and the left and right circular polarization states, could then be plotted, in principle, as LD and CD, respectively. This device was not employed in the analysis of single crystals, but rather in the analysis of polycrystalline biological structures such as intracellular polymeric hemoglobin aligned in subjects burdened by sickle cell anemia.[4] LD and circular differential images[5] were produced also for spermatocyte nuclei. Here, a sample micro-positioning stage was used to make images in conjunction with a photo multiplier tube detector.[6] Bustamante and coworkers introduced an image dissector to scan the image of a sample on a fixed stage, focusing especially on sickled hemoglobin.[7]

By 1995, the use of a linear 1024 diode array was responsible for much greater detail in the LD images, thereby permitting the sub-classification of sickled hemoglobin cells.[8] CD imaging microscopy did not develop in tandem with LD imaging microscopy, the former having been comparatively troublesome. The idea of a CD microscope for anisotropic samples was proposed in 1982 by Maestre and Katz who adapted a Carey spectropolarimeter to a microscope[9] for single point measurements of the CD spectra of chromatin. They faced instrumental artifacts[10] arising from electronic polarization modulators in commercial instruments that typically generate sinusoidally varying polarization states,[11] thereby introducing a small admixture of linearly polarized light into the circularly polarized output. Residual ellipticity, when coupled with the LB and LD of ordered media, generates artifactual CD signals.[12,13] Strain in photoelastic modulators (PEMs) compounds these artifacts.[14] Attempts have been made to skirt these problems by adding additional modulators,[15] rotating the sample,[16] performing complex analytical transformations of independent chiroptical measurements,[17] or choosing components that minimize polarization biases.[18] Nevertheless, a reliable device for imaging CD has eluded investigators for the most part. Recently, CD images of d-camphorsulfonic acid films with a spatial resolution of < 1 μ were obtained by Yamada *et al.*[19] They employed a polarizing undulator applied to near UV synchrotron radiation.

3. Tools

3.1. Jones calculus

A variety of methods have been developed for tracking the polarization state of light as it passes through successive optical elements and complex samples. These are the Poincaré sphere,[20] the Mueller calculus,[21] and the Jones calculus.[22] These tools, and their relative advantages, have been treated in detail elsewhere.[23] Here, we give an overview of the Jones formalism, the only method that we will make use of in the following.

The x and y components of an electric vibration can be represented by a two-element column vector called the Jones vector after its inventor R. Clark Jones. If the amplitudes of the x and y components are given as $A_x e^{i\phi_x}$ and $A_y e^{i\phi_y}$ then the Jones vectors (**J**) for linear polarized light along **x** ($\mathbf{J}_{x\text{-}pol}$), elliptically polarized light ($\mathbf{J}_{ellipt}$), as well as right ($\mathbf{J}_{rcp}$) and left ($\mathbf{J}_{lcp}$) circularly polarized light are:

$$\mathbf{J}_{x-pol} = \begin{bmatrix} A_x e^{i\phi_x} \\ 0 \end{bmatrix} \quad \mathbf{J}_{ellipt} = \begin{bmatrix} A_x e^{i\phi_x} \\ A_y e^{i\phi_y} \end{bmatrix}$$

$$\mathbf{J}_{rcp} = \begin{bmatrix} Ae^{i\phi} \\ Ae^{i(\phi+\pi/2)} \end{bmatrix} \quad \mathbf{J}_{lcp} = \begin{bmatrix} Ae^{i\phi} \\ Ae^{i(\phi-\pi/2)} \end{bmatrix}.$$

The Jones vectors may be normalized such that $\mathbf{J}^*\mathbf{J} = A_x^2 + A_y^2 = 1$. The resulting expressions are invariant to a constant phase added to both components. Thus, simpler equivalent vectors follow:

$$\mathbf{J}_{x-pol} = \begin{bmatrix} 1 \\ 0 \end{bmatrix} \quad \mathbf{J}_{ellipt} = \frac{1}{\sqrt{A_x^2 + A_y^2}} \begin{bmatrix} A_x \\ A_y e^{i\phi_y} \end{bmatrix}$$

$$\mathbf{J}_{rcp} = \frac{1}{\sqrt{2}} \begin{bmatrix} 1 \\ i \end{bmatrix} \quad \mathbf{J}_{lcp} = \frac{1}{\sqrt{2}} \begin{bmatrix} 1 \\ -i \end{bmatrix}.$$

Given an input polarization state, $\mathbf{J}_{in}$, the output polarization state, $\mathbf{J}_{out}$, can be reckoned with a square matrix (**M**) that represents the sample, or some optical element such that:

$$\mathbf{J}_{out} = \mathbf{M}\,\mathbf{J}_{in}$$

The matrices corresponding to a linear polarizer along **x**, an arbitrary retardation plate inducing a phase shift $\delta = 2\pi L\Delta n/\lambda$ (L is the sample thickness, Δn is the birefringence and λ is the wavelength) of the emergent light, and a linear polarizer

oriented at an arbitrary angle θ are:

$$\mathbf{M}_{x-pol}=\begin{bmatrix}1 & 0\\ 0 & 0\end{bmatrix}\quad \mathbf{M}_{retard}=\begin{bmatrix}e^{i\delta/2} & 0\\ 0 & e^{-i\delta/2}\end{bmatrix}$$

$$\mathbf{M}_{\theta-pol}=\mathbf{R}_\theta^T\mathbf{M}_{x-pol}\mathbf{R}_\theta=\begin{bmatrix}\cos^2\theta & \sin\theta\cos\theta\\ \sin\theta\cos\theta & \sin^2\theta\end{bmatrix},$$

$$\mathbf{R}_\theta=\begin{bmatrix}\cos\theta & \sin\theta\\ -\sin\theta & \cos\theta\end{bmatrix}$$

Below, the Jones formalism is used to construct right circularly polarized light from a quarter wave plate acting on linearly polarized light oriented at 45° with respect to the eigen modes of the wave plate. A constant phase has been added to simplify the expression.

$$\mathbf{J}_{out}=\begin{bmatrix}e^{i\pi/4} & 0\\ 0 & e^{-i\pi/4}\end{bmatrix}\mathbf{R}_{45}\begin{bmatrix}1\\0\end{bmatrix}=\begin{bmatrix}e^{i\pi/4} & 0\\ 0 & e^{-i\pi/4}\end{bmatrix}\frac{1}{\sqrt{2}}\begin{bmatrix}1\\-1\end{bmatrix}$$

$$=\frac{1}{\sqrt{2}}\begin{bmatrix}e^{i\pi/4}\\ -e^{-i\pi/4}\end{bmatrix}\equiv\frac{1}{\sqrt{2}}\begin{bmatrix}e^{i\pi/4-i\pi/4}\\ -e^{-i\pi/4-i\pi/4}\end{bmatrix}=\frac{1}{\sqrt{2}}\begin{bmatrix}1\\ i\end{bmatrix}=\mathbf{J}_{rcp}$$

3.2. Metripol

In order to quantify linear anisotropies we have employed the rotating polarizer technique as embodied in the Metripol microscope.[24] The optical train consists of a filter as monochrometer, a mechanically rotating polarizer, a sample inducing the phase shift δ, a quarter wave retarder and a polarizer aligned at 45° towards the quarter wave plate's eigen ray directions:

$$\mathbf{A}' = \mathbf{M}_{45\text{-}pol}\mathbf{M}_{\lambda/4}\mathbf{M}_{sample}\mathbf{R}_\theta\mathbf{J}_x$$

The position of the sample with respect to the rotating polarizer is defined by the angle θ, $\theta = \alpha - \phi$, where α is the rotation angle of the polarizer and ϕ the angle between the slow vibration direction of the sample and the polarizer when $\alpha = 0$.

The amplitude of the emergent light form A' is then given as:

$$A'=\frac{1}{2}\begin{bmatrix}1 & 1\\ 1 & 1\end{bmatrix}\cdot\begin{bmatrix}e^{i\frac{\pi}{4}} & 0\\ 0 & e^{-i\frac{\pi}{4}}\end{bmatrix}\cdot\begin{bmatrix}e^{i\frac{\delta}{2}} & 0\\ 0 & e^{-i\frac{\delta}{2}}\end{bmatrix}\cdot\begin{bmatrix}\cos\theta & \sin\theta\\ -\sin\theta & \cos\theta\end{bmatrix}\cdot$$

$$\begin{bmatrix}1\\0\end{bmatrix}=\frac{1}{2}\begin{bmatrix}\cos\theta e^{ix}-\sin\theta e^{-ix}\\ -\sin\theta e^{-ix}+\cos\theta e^{ix}\end{bmatrix}_{x=(\frac{\delta}{2}+\frac{\pi}{4})}$$

From the amplitudes, the normalized intensity I/I_0 is found directly as:

$$\frac{I}{I_0}=A'^{*}\cdot A'=2\cdot\frac{1}{4}\left[\left(\cos\theta\, e^{ix}-\sin\theta\, e^{-ix}\right)\left(\cos\theta\, e^{-ix}-\sin\theta\, e^{ix}\right)\right]$$

$$=\frac{1}{2}\left[\cos^2\theta-\cos\theta\sin\theta\left(e^{2ix}+e^{-2ix}\right)+\sin^2\theta\right]$$

$$=\frac{1}{2}\left[1-\cos\theta\sin\theta\,2\cos(2x)\right]$$

$$=\frac{1}{2}\left[1+\sin 2\theta\sin\delta\right]$$

$$=\frac{1}{2}\left[1+\sin 2(\alpha-\phi)\sin\delta\right]$$

Fig. 1 shows how the intensity varies as a function of the polarizer angle and the parameters δ and ϕ.

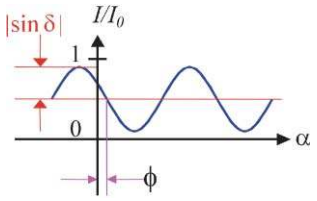

Fig. 1 Dependence of signal I/I_0 on the rotation of the polarizer angle (α). The amplitude is related to the phase difference (δ), the phase shift gives the optical orientation (ϕ), and the offset gives the transmittance.

In earlier incarnations of the rotating polarizer technique,[25] the phase velocity was taken to be $\alpha = \omega t$. This latter description, however, was incompatible with CCD imaging in which each pixel must be computed independently. In the Metripol method, intensity measurements at discrete steps (α_i) generate expressions that are easily converted to linear polynomials. Data collected over full periods yield Fourier coefficients from which the variable parameters are extracted analytically without any computationally intensive matrix inversions.

Simple modifications of the optical train permit the measurement of LD and of OR in special cases. The anisotropic absorption may be experimentally accessed by removing the quarter wave plate and analyzer. The resulting optical train is represented by:

$$\mathbf{A}'=\mathbf{M}_{sample}\mathbf{R}_\theta\mathbf{J}_x,\ \mathbf{M}_{sample}=\begin{bmatrix}t_x e^{i\delta/2} & 0\\ 0 & t_y e^{-i\delta/2}\end{bmatrix}t$$

$$t=e^{\frac{1}{4}(a_x+a_y)}\qquad t_{x/y}=e^{\pm\frac{\varepsilon}{2}}$$

$(tt_x)^2$ and $(tt_y)^2$ are the transmission coefficients of the sample along the eigen ray directions. $\varepsilon = (\mathbf{a}_x - \mathbf{a}_y)/2$ where $a_{x/y}$ are the absorption coefficients. Applying the same procedure as before, neglecting overall absorption, t^2, we find an expression for the intensity that is independent of δ:

$$\frac{I}{I_0}=t_x^2\cos^2\theta+t_y^2\sin^2\theta,$$

which may be recast in the more useful form:

$$\frac{I}{I_0}=\frac{1}{2}\left(t_x^2+t_y^2\right)+\frac{1}{2}\left(t_x^2-t_y^2\right)\cos(2\theta).$$

$$\frac{I}{I_0}=\cosh\varepsilon+\cos(2\theta)\sinh\varepsilon,$$

or

$$\frac{I/I_0}{\cosh\varepsilon}=1+\cos(2\theta)\tanh\varepsilon.$$

In a measurement, the detected intensities, I, are normalized to the average intensities, $I' = I/\langle I\rangle$.

$$\frac{I'}{I_0}\equiv[1+\cos(2\theta)\tanh\varepsilon].$$

The amplitude in Fig. 1 is then determined by tanh ε, a measure of the scaled differential transmission, or LD.

A second variation in the optical train can be used to probe optically active materials in the absence of birefringence, requiring only the removal of the quarter wave plate:

$$\mathbf{A}'=\mathbf{M}_{pol-y}\mathbf{M}_{sample}\mathbf{R}_\theta\mathbf{J}_x=\begin{pmatrix}0\\ -\sin\theta\end{pmatrix}.$$

In this case, $\mathbf{M}_{sample}$ is the unit matrix and the only

non-vanishing component of $\mathbf{M}_{pol\text{-}y}$ is $M_{22} = 1$, giving the intensity expression:

$$\frac{I}{I_0} = \sin^2\theta = \frac{1}{2}(1 - \cos 2\theta).$$

3.3. HAUP and S-HAUP

To measure OR (circular birefringence, $\Delta n_{CB} = n_R - n_L$) along a general direction of a crystal one must deconvolve the influence of LB ($\Delta n_{LB} = n'' - n'$). Although the *intensity* of light passing through a polarizer, chiral anisotropic sample, and analyzer contains the necessary information for extracting OR, implementation of this idea prior to the invention of electrophotometry and stable, high-intensity light sources was impossible. For generations, most researchers conceded that measuring OR in the presence of large LB was not a realistic goal.

In 1983, Uesu and Kobayashi pushed through this impasse by using lasers, photon counting, and computerized modulation of polarizer and analyzer orientations to determine OR in crystals for directions off the optic axes.[26] They called this experiment HAUP (high accuracy universal polarimetry) whose basic geometry is given in Fig. 2. Since we apply the

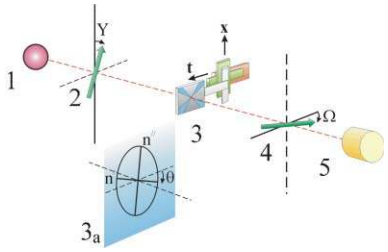

Fig. 2 The HAUP optical train. (1) light source, (2) polarizer, rotation angle Y, (3) sample and translation stage with translation directions t and x, (3a) extinction angle θ of the birefringent cross-section with refractive indices n' and n'', (4) analyzer, rotation angle Ω, (5) detector.

HAUP technique to heterogeneous crystals, the polarimeter was fitted with a translation stage in order to produce topographs of the optical parameters. In this way, maps were made comprising 100 × 100 pixels at a resolution of about 30 μm per pixel. In the Fourier analysis of the intensity data, the apparent extinction angle convolved with circular dichroism ($\theta(\theta_0, \eta)$), the phase factor (δ), and the apparent OR (φ) were unfolded. We call the imaging experiment scanning-HAUP (S-HAUP).

According to the Jones-matrix formalism,[27] a sample that shows LB ($\delta = 2\pi\Delta n_{LB}L/\lambda$) and OR ($\varphi$), as well as CD ($\eta$) is given by the following:

$$\mathbf{M}(\delta,\varphi,\eta) = \begin{bmatrix} e^{i\delta/2} & -2(\varphi + i\eta)\dfrac{\sin(\delta/2)}{\delta} \\ 2(\varphi + i\eta)\dfrac{\sin(\delta/2)}{\delta} & e^{-i\delta/2} \end{bmatrix}.$$

In a HAUP experiment, the sample at extinction angle θ_0 is placed between two orthogonal polarizers, which are rotated about small angles Y and Ω (Fig. 2). The optical train is represented by a string of matrices yielding the light amplitude $\mathbf{A}$ from the rotation matrices for the polarizer ($\mathbf{R}_Y$), analyzer ($\mathbf{R}_\Omega$), and sample ($\mathbf{R}_{\theta_0}$):

$$\mathbf{A} = \mathbf{R}_\Omega^T \begin{bmatrix} 0 & 0 \\ 0 & 1 \end{bmatrix} \mathbf{R}_\Omega \mathbf{R}_{\theta_0}^T \mathbf{M} \mathbf{R}_{\theta_0} \mathbf{R}_Y \begin{bmatrix} 1 \\ 0 \end{bmatrix},$$

with

$$R_\Omega = \begin{bmatrix} \cos\Omega & -\sin\Omega \\ \sin\Omega & \cos\Omega \end{bmatrix}, \quad R_Y = \begin{bmatrix} \cos Y & -\sin Y \\ \sin Y & \cos Y \end{bmatrix},$$
$$R_\theta = \begin{bmatrix} \cos\theta_0 & -\sin\theta_0 \\ \sin\theta_0 & \cos\theta_0 \end{bmatrix}.$$

The result of these operations is written approximately as a bi-quadratic polynomial that is normalized to the amplitudes of Y^2 and Ω^2:

$$\frac{I}{I_0} = A^* \cdot A = a_0 + a_1\Omega + a_2 Y + a_3\Omega Y + \Omega^2 + Y^2,$$

with

$$\frac{1}{2}a_1 = -\theta(\delta) + \varphi(\delta) = (\theta_0 - \frac{\eta}{\delta})(\cos\delta - 1) + \frac{\varphi_0}{\delta}\sin\delta,$$

$$\frac{1}{2}a_2 = \theta(\delta) + \varphi(\delta) = (\theta_0 - \frac{\eta}{\delta})(1 - \cos\delta) + \frac{\varphi_0}{\delta}\sin\delta,$$

$$\frac{1}{2}a_3 = \cos\delta.$$

The first term (a_0) is the overall offset in the intensity measurement. Parameters φ and θ are found from combinations of the parameters a_i: $\varphi \times ((\sin\delta)/\delta) = (a_1 + a_2)/4$; $\theta(\theta_0, \eta) \times ((\cos\delta) - 1) = (a_2 - a_1)/4$.

3.4. Circular extinction imaging

Reasonable sensitivity in CD measurements is commonly achieved by rapid sampling concomitant with electronic light modulation at rates of 50–100 kHz. Why then not add contemporary CCD detection to make CD images? Operating at less than 1 kHz, CCDs are incompatible with PEMs. While others are trying to force compatibility[28] by speeding up the CCD[29] or slowing down the modulation,[30] these designs remain constrained by limited spectral ranges, noise, and parasitic ellipticities.[31] On the other hand, physicists recently built single point CD spectropolarimeters for anisotropic media *via* schemes using mechanical light modulation with photo multiplier tubes as detectors.[32] Their devices were extremely slow but nevertheless suited to large, homogeneous, strong circularly dichroic crystals.

We built a circular dichroism imaging microscope (CDIM) based on the apparently retrogressive mechanical modulation of near perfect circularly polarized light (CPL) in conjunction with CCD detection (Fig. 3). Signal to noise lost in slow

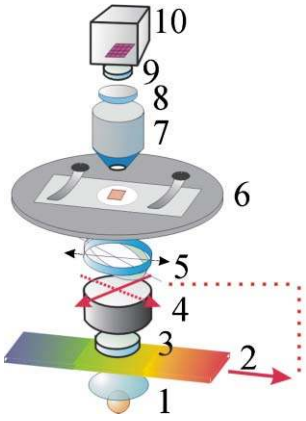

Fig. 3 Visible light circular dichroism imaging microscope (CDIM). Schematic omits motors and mounts. (1) light source, (2) variable interference filter, (3) depolarizer, (4) rotating polarizer, (5) tilting $\lambda/4$-compensator, (6) sample mount, (7) objective, (8) projector lens, (9) depolarizer, (10) CCD-camera.

modulation (< 30 Hz) is regained by signal averaging with a CCD camera. We abandoned the use of a broad band $\lambda/4$ plate in favor of a variable retarder that is adjusted so that it functions as a perfect $\lambda/4$ plate at each wavelength.

The Jones matrix for a birefringent and circular dichroic sample is:[12]

$$\mathbf{M}(\delta,\eta) = \begin{bmatrix} e^{ix} & i\eta\dfrac{\sin x}{x} \\ -i\eta\dfrac{\sin x}{x} & e^{-ix} \end{bmatrix}$$

where $x = \delta/2$, and the CD is defined as $\eta = 4(I_+ - I_-)/I_0$, where I_+ and I_- are right and left CPL, respectively. The complex vectors A represent these light forms, where E_0 is the amplitude of the incoming light wave.

The intensity $I'_\pm$ is found from $A_\pm{}'^{*} \cdot A_\pm{}'$, where $A_\pm{}' = \mathbf{M}\,A_\pm$. The total intensity is then:

$$\frac{I'_\pm}{E_0^2} = 1 \pm 2\eta\frac{\sin x\cos x}{x} + \eta^2\frac{\sin^2 x}{x^2}$$

The normalized intensity difference in a birefringent sample then is found as:

$$\frac{I'_R - I'_L}{I_0} = 4\eta\frac{\sin x\cos x}{x} = 4\eta\frac{\sin\delta}{\delta}.$$

This expression describes the observed CD in a birefringent sample provided that there is no parasitic linearly polarized contribution to the incoming CPL.

4. Applications

4.1. Linear birefringence

Metripol was applied in its inaugural publication[23] to the ferroelectric perovskite $BaTiO_3$, synthetic diamond, and anorthosite. In $BaTiO_3$, tetragonal domains showed stress birefringence when high-temperature cubic crystals were cooled to room temperature. Synthetic diamond showed stress birefringence associated with defects and growth sector boundaries. One of these celebrated images now graces the cover of the volume of the *International Tables for Crystallography* devoted to physical properties.[33] The anorthosite micrographs dramatically show the twin laws common to plagioclases. More recent crystallographic applications of Metripol include illustrations of the relaxor ferroelectric $Na_{1/2}Bi_{1/2}TiO_3$,[34] and of phase transitions in $Pb(Mg_{1/3}Nb_{2/3})_{(1-x)}Ti_xO_3$[35] and $K_2Mn_2(SO_4)_3$.[36] Hollingsworth and Peterson used Metripol to demonstrate domain switching in ferroelastic pseudo-hexagonal crystals of 2,10-undecanedione.[37]

4.1.1. K_2SO_4. A simple application and illustration of Metripol is the screening of birefringent crystals. Shown in Fig. 4 are three micrographs of the simple salt, K_2SO_4, grown from aqueous solution on a glass slide. Fig. 4a shows the phase difference between the two eigenmodes propagating through the birefringent, orthorhombic crystals (space group *Pmcn*) plotted as $|\sin\delta|$ in false color. $|\sin\delta|$ is naturally a periodic function, but since K_2SO_4 is weakly birefringent and the crystals are thin, the arc sine can be taken as the true value of the phase factor. This micrograph is independent of crystal orientation with respect to the coordinate system of the microscope. In an ordinary petrographic microscope, the intensity of the transmitted light depends not only on the intrinsic retardation but on the orientation of the individual crystallites.

In Fig. 4b, the orientations of cross sections of the optical indicatrices are given as the angle of the slowest vibration direction (the largest refractive index) measured counterclockwise from the horizontal axis. Here, one can plainly see

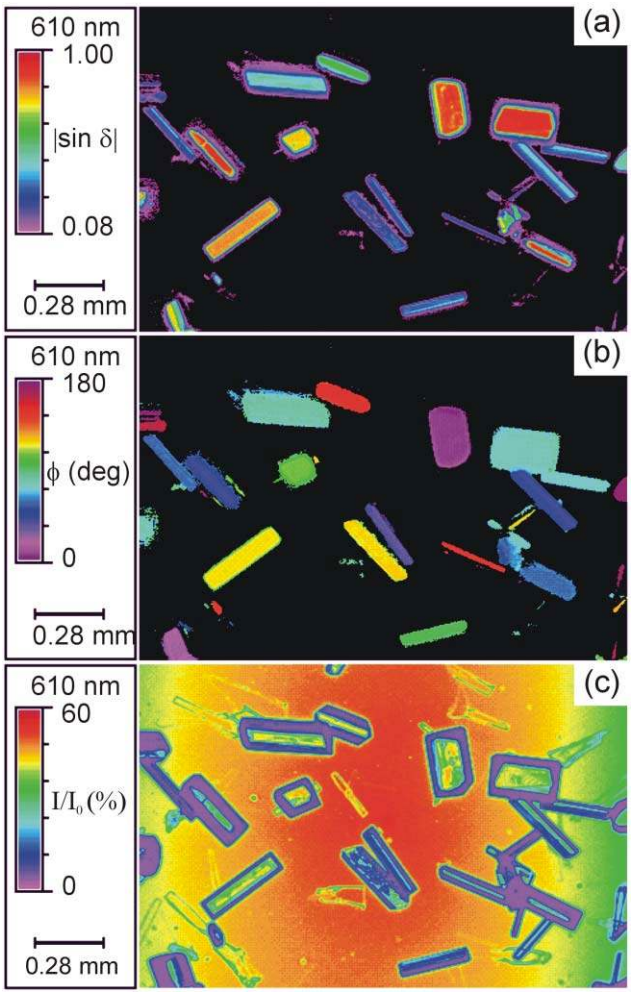

Fig. 4 Metripol micrographs of K_2SO_4 crystallites. (a) $|\sin\delta|$, (b) ϕ (deg), (c) I/I_0 (%).

that the needles have distinct presentations. Some crystals are lying on (010) whereas others are lying on (021). The two "yellow crystals" in Fig. 4b must have different presentations as the [100] needles are pointing in orthogonal directions: the only way they can both give the same false color is if the fast and slow axes with respect to the microscope have been inverted. It is easy to distinguish in the transmission map in Fig. 4c those rectilinear crystals sitting on (010) from those with oblique (021) presentations. The non-transmissive "purple" edges in Fig. 4c are merely inclined.

4.1.2. $NaCl_xBr_{1-x}O_3$. Naturally, cubic crystals are optically isotropic, but they can become birefringent when grown in the presence of impurities that can reduce their symmetry[38] either by selectively occupying sites on growing surfaces that have distinct presentations or by exerting stresses that can influence the optical properties *via* the photoelastic, or piezo-optic effects. In an ordinary polarizing microscope the birefringence makes itself evident in complex patterns of interference colors.[39] Metripol analysis of slices can parse the various contributions to these ordinary micrographs.

A classic example of such so-called optically anomalous crystals[40] is a mixture of $NaClO_3$ and $NaBrO_3$. The cubic salts are miscible in all proportions in the solid state. Mixed crystals have cube {100} habits unless the mole fraction of BrO_3^- is greater than 0.95 at which point the crystals become tetrahedral. The {111} crystals can be prepared by modifying the habit in the presence of $S_2O_3^{2-}$ (Fig. 5). Shown in Fig. 6 are thin sections of mixed crystals of $NaCl_xBr_{1-x}O_3$ that are

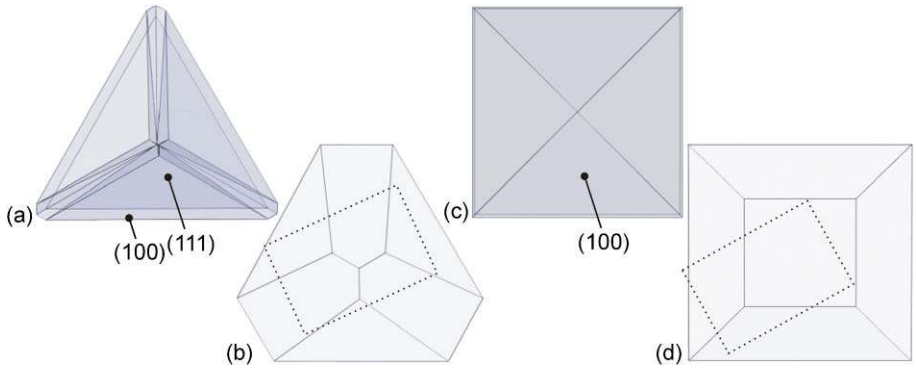

Fig. 5 Tetragonal and cubic habits of the sodium halates along with slices that indicate the bisected growth sectors. Dotted regions demarcate areas represented in micrographs in Fig. 6. All of the crystal drawings herein were prepared by WinXMorph (W. Kaminsky, 2004).[41]

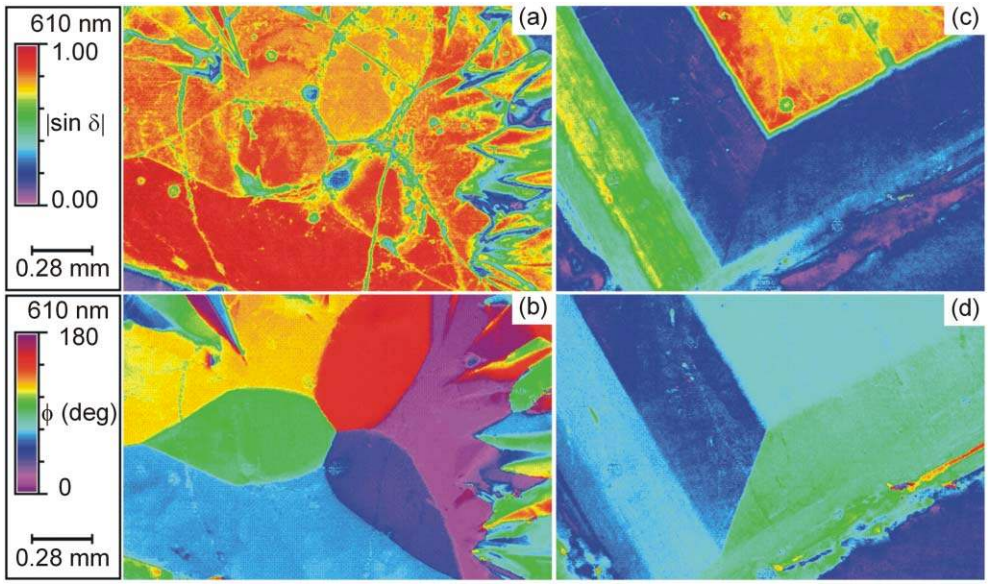

Fig. 6 Metripol LB micrographs of the sodium halates. (a,c) |sin δ| maps. (b,d) Extinction maps. Orientation is measured counterclockwise from the horizontal axis. (a,b) $NaCl_{0.50}Br_{0.50}O_3$ grown in the presence of 5% $Na_2S_2O_3$, 91 μm. (c,d) $NaCl_{0.87}Br_{0.13}O_3$, 98 μm.

presented along a 3-fold crystallographic axis in {111} crystals and the 2-fold crystallographic axis in {100} crystals (referred to the idealized cubic system, space group $P2_13$). The birefringence is evident in the |sin δ| maps, Figs. 6a and 6c. The corresponding extinction maps are shown in Figs. 6b and 6d. In the cubes, the central section represents a {100} sector viewed along the growth direction. It has a much greater birefringence than the surrounding regions that represent sectors viewed normal to the growth directions. Despite these large differences in the LB there is little difference in extinction. In the tetrahedral crystals, the magnitude of |sin δ| varies slightly but chaotically across the crystal plate. Nevertheless, the construction of the assemblage shows up brilliantly in the orientation image (Fig. 6b) where there are trigonal arrangements of three {100} and three {111} sectors. The tear-shaped {100} sectors indicate a changing habit from {100} to {111} in the presence of $S_2O_3^{2-}$. A complete interpretation of these images requires further separation of the chiroptical properties that can not be accomplished in a birefringent crystal with Metripol alone (Section 4.3.1).

4.1.3. 1,8-Dihydroxyanthraquinone. Another example of an optically anomalous crystal is 1,8-dihydroxyanthraquinone (**1**, Fig. 8). The crystals form square plates and are well-refined in the space group $P4_{1(3)}$; they should not be birefringent when viewed along the optic axis. However, the crystals display complex patterns of birefringence as shown in Fig. 7a. Despite the variance in |sin δ| across the crystal plate, the extinction is relatively simple, indicating biaxial sectors related to one another by 90° rotations. Here again, by itself, Metripol did not aid in our understanding of the apparent reduction in optical symmetry. A deeper analysis requires the incorporation of chiroptical effects (Sections 4.3.1/4.5.1).

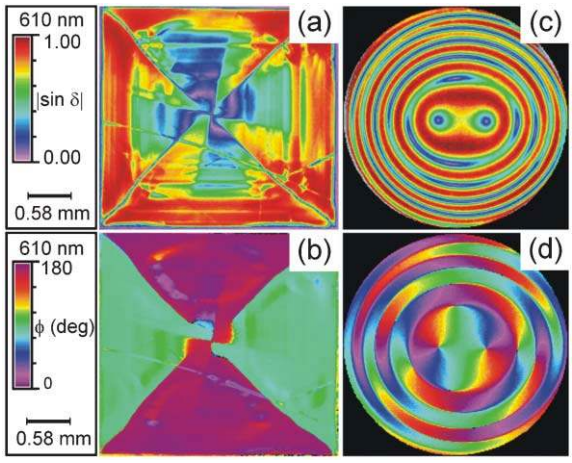

Fig. 7 Metripol LB micrographs of 1,8-dihydroxyanthraquinone (**1**). (a,b) orthoscopic illumination. (c,d) conoscopic illumination. (a,c) |sin δ| (b,d) ϕ(deg).

The new methods of analysis work equally well in conoscopic as well as orthoscopic illumination.[42] The conoscopic image corresponding to the |sin δ| map (Fig. 7c) shows the birefringence increasing from the positions of the optic axes (central nodes). Moving outward, |sin δ| passes at least four successive minima and maxima. The orientation image shows alternating bands with 90° relationships between adjacent bands. This is a consequence of the fact that the intensity formula at a fixed wavelength results in an ambiguity in the relationship between |sin δ| and ϕ; each time |sin δ| passes through zero, the calculated ϕ undergoes a 90° phase shift. The helical nature of the orientation map (Fig. 7d) is a manifestation of the so-called Airy's spiral in a biaxial crystal.[43] Geday and Glazer showed that in a uniaxial crystal the magnitude of the optical rotation about the optic axis can be read directly from the conoscopic orientation image by measuring the inclination of $\phi = \theta(\phi_0)$.[42] For small rotations (ρ), it was shown that the inclination of the zero orientation was proportional to $-1/2\rho L$ where L is the thickness. Whether this approximation is valid for biaxial, circularly dichroic samples is a matter for further investigation.

4.2. Linear dichroism

4.2.1. 1,8-Dihydroxyanthraquinone. The tetragonal form of 1,8-dihydroxyanthraquinone (**1**; Fig. 8) displays anomalous LB

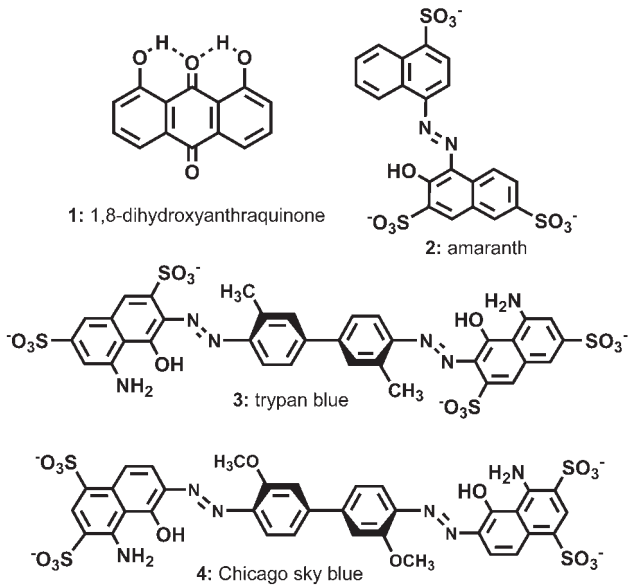

Fig. 8 Dyes.

but not anomalous LD. The square plates precipitate simultaneously with an orthorhombic polymorph (space group $Pca2_1$) having hair-like needle habits. These needles must be linearly dichroic, and indeed, the dichroism and the orientation of the most strongly absorbing direction can be displayed as false color maps with Metripol as in Figs. 9a and 9b. This is achieved by choosing a filter that passes monochromatic light in the absorption band of the crystal and by removing the circular analyzer as described above (Section 3.2).

4.2.2. Dyed K_2SO_4. In the same way that linear birefringence can be produced in crystals of $NaClO_3$ or $NaBrO_3$ through mutual admixing, colorless crystals such as K_2SO_4 can be made linearly dichroic by including in the growth solution dyes that are oriented and overgrown by the transparent host. In this way, we obtain dyes in single crystal register, uncomplicated, in many cases, by the collective interactions that

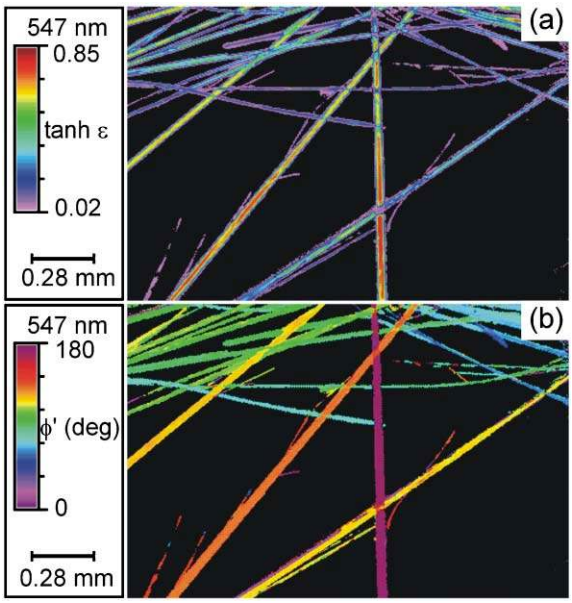

Fig. 9 LD micrographs of the metastable, orthorhombic polymorph of 1,8-dihydroxyanthraquinone. (a) tanh ε, (b) ϕ' (deg).

frequently occur in dye single crystals. We have made an extensive study of the process of dyeing crystals,[44] especially K_2SO_4.[45]

The dye amaranth (**2**) stains the {110} and {010} growth sectors of K_2SO_4 (Fig. 10). The tanh ε image (Fig. 11a) shows

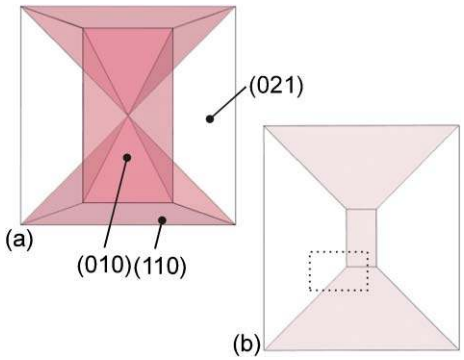

Fig. 10 Schematic of an amaranth dyed K_2SO_4 crystal. (a) Crystal as grown, (b) (010) slice.

that the magnitude of the absorption anisotropy is comparable in the two sectors - though greater in the center of {010} suggesting that rapid early growth leads to higher anisotropy, a likely consequence of a selective, kinetically controlled process – while the anisotropy disappears near the intersection of the sectors. Since the dye adopts orthogonal orientations in the two sectors (Fig. 11b), the regions of overlap in a crystal of finite thickness lead to isotropic absorption.

4.3. Circular birefringence

The first topograph of optical rotation measured along a birefringent direction in a crystal was of the mineral langbeinite, $K_2Cd_2(SO_4)_3$.[46] This was achieved *via* a modification of the S-HAUP technique that also involves a birefringence modulation by tilting the crystal about an axis perpendicular to the wave vector. However, given the time-consuming measurement process requiring successive scanning and tilting, the resolution of the image was low. Topographs of the spontaneous Faraday effect in $FeBO_3$ were produced shortly thereafter by making measurements below the Curie

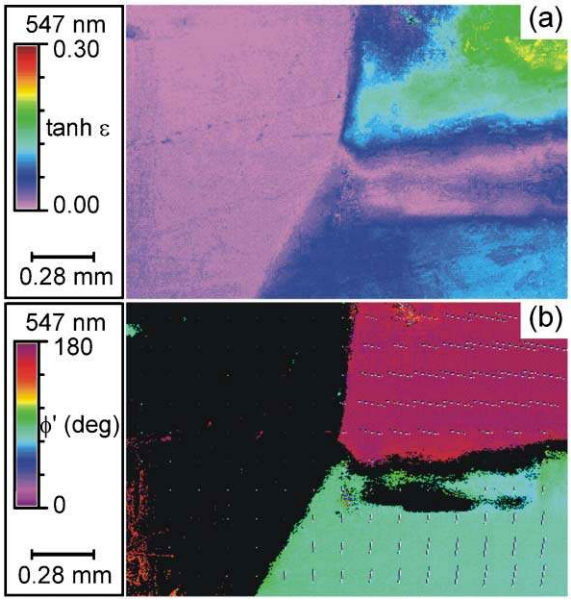

Fig. 11 Metripol LD micrographs of amaranth (**2**) dyed K_2SO_4. (a) tanh ε, (b) ϕ' (deg). Orientation azimuths have been plotted on micrograph.

temperature.[47] Both positive and negative optically rotatory domains were revealed in topographs of triglycine sulfate $[(NH_2CH_2COOH)_3{\cdot}H_2SO_4]$.[48]

Along non-birefringent crystallographic directions, Metripol can be used to image optical rotation directly. A reduced optical path is employed in which only the quarter wave plate is removed. This is illustrated for the case of a (0001) slice of quartz. Quartz crystals are usually marked by Dauphine twins related by a 180° rotation about the hexagonal axis, and Brazil twins where dextro- and levorotatory domains are reflected across {11-20}, such as those in Fig. 12.

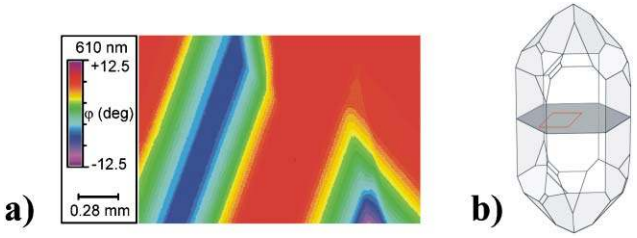

Fig. 12 Enantiomorphous Brazil twinning in a (0001) plate of quartz. (a) Optical rotation plotted as φ(deg). (b) Idealized representation of quartz crystal and the slice from which the micrograph was made.

4.3.1. $NaCl_xBr_{1-x}O_3$. $NaClO_3$ and $NaBrO_3$ have long puzzled crystallographers. Imagine Marbach's consternation when in 1856 he observed that levorotatory crystals of $NaClO_3$ nucleated dextrorotatory crystals of its isomorph $NaBrO_3$ and *vice versa*.[49] Bijvoet and coworkers[50] ultimately established on the basis of the anomalous dispersion of X-rays that homochiral crystals of $NaClO_3$ and $NaBrO_3$ do indeed have opposite signs of optical rotation. Why?

An experiment that might lend some insight into this problem would exploit the miscibility of the two halates to determine whether the contributions from the components to the rotatory power were independent of one another. This question has not been addressed because the mixed crystals display the anomalous birefringence described in Section 4.1.2 that precluded measurements of optical rotation. Annealing near the melting temperature can remove the anomalous birefringence and restore $P2_13$ symmetry. Several groups have measured the rotation in isotropic, annealed mixed crystals but with compositions exceeding no more than 15% bromate,[51] thus only a small part of the mixed crystal space was analyzed in crystals in which information encoded during growth was destroyed. We have studied the development of LB in the mixed crystals across the entire composition range in some detail but OR had been out of reach.[52]

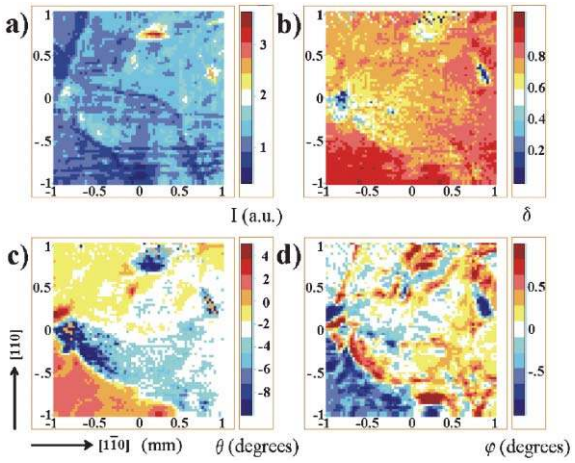

Fig. 13 S-HAUP generated topographs of optical properties of a mixed halite ($NaCl_{0.5}Br_{0.5}O_3$, 0.435 mm thick) crystal. (a) transmission (arbitrary units, a.u.), (b) phase difference δ, (c) extinction θ(deg), (d) optical rotation φ(deg).

In order to image OR along birefringent directions, S-HAUP is required. Shown in Figs. 13a–d are four S-HAUP topographs displaying the separation of the transmission, retardation, extinction, and optical rotation of a mixed halate crystal. The as-grown crystal topographs are chaotic. The presence of dextro- and levorotatory domains may indicate the segregation of BrO_3^- and ClO_3^- on the microscale.

4.3.2. 1,8-Dihydroxyanthraquinone. Tetragonal crystals of 1,8-dihydroxyanthraquinone (**1**) were examined by the S-HAUP method. They appeared to have both dextro- and levorotatory domains (Fig. 14c), however, the poor quality of

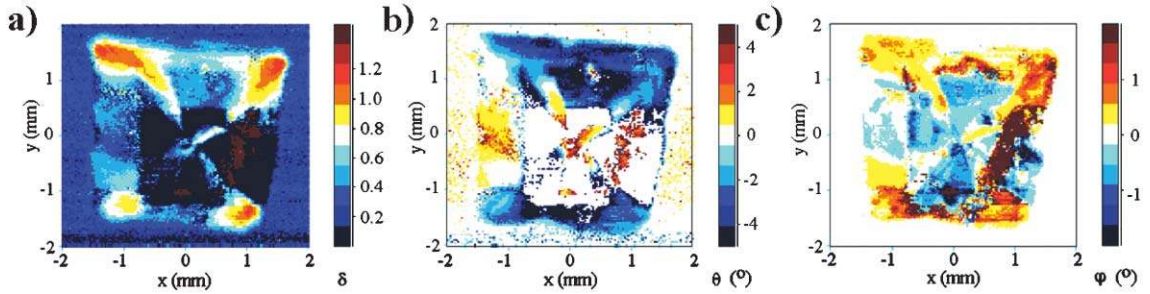

Fig. 14 S-HAUP topographs of 1,8-dihydroxyanthraquinone. (a) Phase difference δ; (b) Extinction θ(deg); (c) Optical rotation φ(deg).

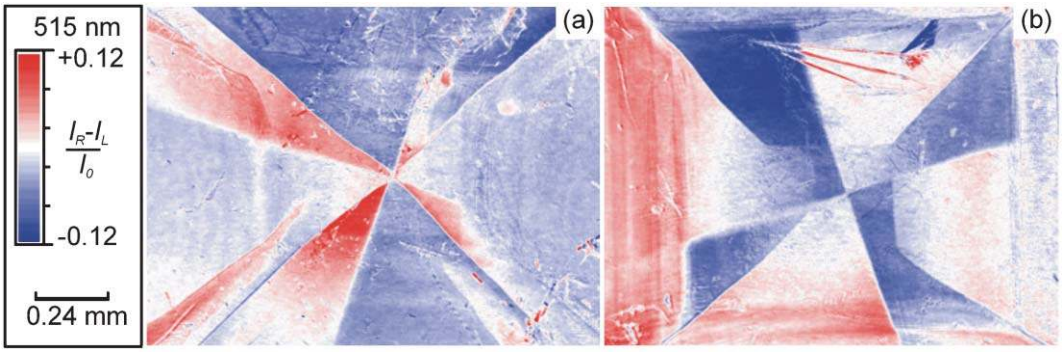

Fig. 15 CD micrographs of the tetragonal form of 1,8-dihydroxyanthraquinone. (a) and (b) are different crystals.

the images, resulting from non-uniform extinction across the crystal plate, made interpretation of the heterochiral domains speculative. Clearly, another tool would be required to further explore this contrast (Section 4.4).

4.4. Circular dichroism: 1,8-dihydroxyanthraquinone

CD imaging is well suited for studying the bright orange crystals of 1,8-dihydroxyanthraquinone (**1**). From our S-HAUP micrographs, we suspected that stress from enantiomorphous twinning resulted in the observed anomalous birefringence. Indeed, CD micrographs in Fig. 15, recorded at 530 nm, show mirror image domains as red (CD is positive) and blue (CD is negative) heterochiral pinwheels. These images are independent of the orientation of the microscope stage, which is the surest way to rule out linear biases in the optical train.

4.5. Anomalous azimuthal rotation and anomalous circular extinction

4.5.1. Dyed K_2SO_4. We set out to use the S-HAUP technique for imaging optical rotation (OR) in simple centrosymmetric crystals that had adsorbed, oriented, and overgrown chiral dye molecules. Chiroptical effects such as OR and CD were expected when equilibrium racemic mixtures of dyes selectively recognized chiral facets of achiral crystalline hosts.

Crystals of K_2SO_4 grown in the presence of trypan blue (**3**) were colored in the {110} and {111} growth sectors. The {111} faces are unusual in the D_{2h}-symmetric crystals because they are chiral. As such, the biaryl dye must be adsorbed enantioselectively to these faces. An idealized drawing of such a dyed crystal is shown in Fig. 16.

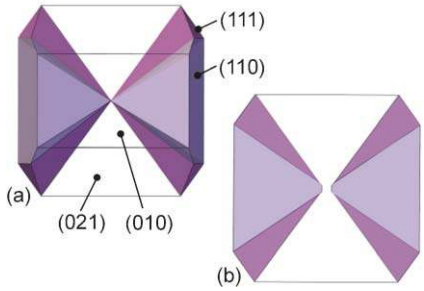

Fig. 16 Schematic of a trypan blue (**3**) dyed K_2SO_4 crystal. (a) Crystal as grown, (b) (010) slice.

S-HAUP topographs of a K_2SO_4/**3** (010) section are shown in Fig. 17, where the dyed regions exhibit contrasting signals consistent with crystal symmetry. The first row in Fig. 17 represents the phase δ, which changes sign when the fast and slow axes are exchanged. In the second row, contrary to expectation, the sign of the apparent OR φ changes with sample

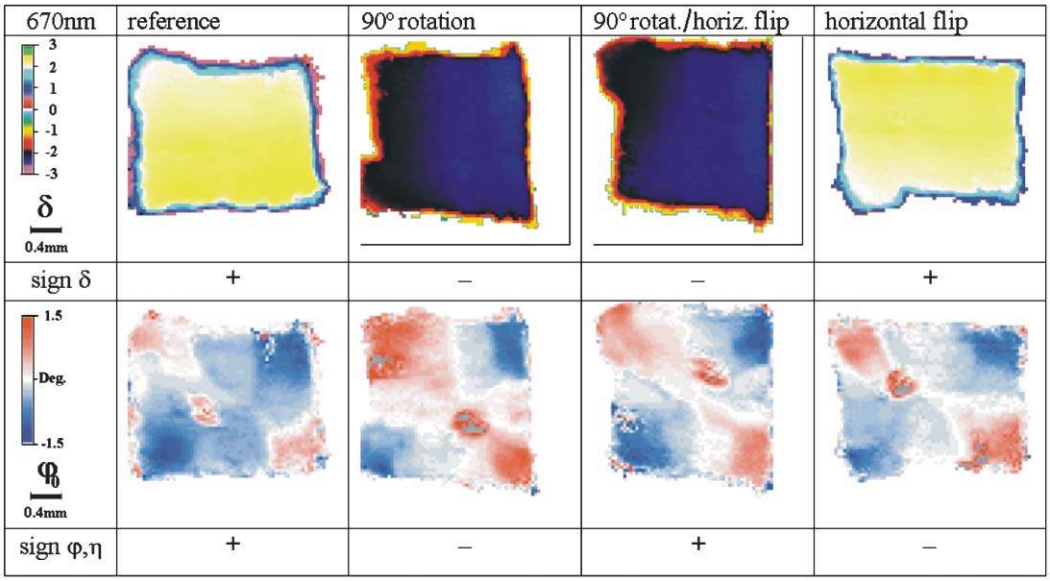

Fig. 17 Optical topographs of K_2SO_4/**3** (010) plate ($\sim$90 μm) using the S-HAUP technique. First row: Phase difference δ, λ = 670 nm for various crystal orientations. The shape of the sample seen in the images in this row is a guide for the eye as the sample is reoriented in the columns of this table. Second row: Apparent optical rotation φ. The signs of the quantities refer to the top-left quadrant in the first image. "Rotation" = 90° rotation about wave vector. "Flip" = 180° rotation about horizontal or vertical axes of the crystal plate.

reorientation, that is, the sign of the effect changes whenever the sample is turned by 90° about the wave vector ("rotation") or rotated 180° around the vertical or horizontal axes perpendicular to the wave vector ("flip"). Intrinsic OR (and CD) would be invariant to these transformations.

What are the origins of the signals in Fig. 17? Dye molecules absorb light anisotropically. In an isotropic medium or along the optic axis of an anisotropic crystal, the absorbance (α) along the induced dipole of the dye affects the electric field component along the dipole according to $(10^{-\alpha})^{1/2}$. The Jones matrix describing the anisotropic absorption of a dipole in its own reference system with the absorption strongest along the y-axis and zero along the x-axis of a Cartesian reference system is then:

$$\mathbf{M}_{Absorption}^{Dipole} = \begin{bmatrix} 1 & 0 \\ 0 & 10^{-\alpha/2} \end{bmatrix}.$$

In an anisotropic host in a birefringent direction, the absorption can only be measured along the eigenmodes e′ and e″ (Fig. 18). If the dye molecules are inclined to e″ of the

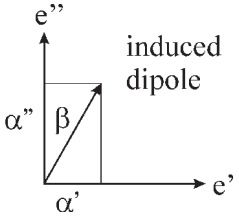

Fig. 18 Projection of the absorption of a dipole on the eigenmodes of a crystal.

host by an angle β, the projections of absorption, α' and α'', on the eigenmodes leads to LD. The angle β is obtained from

$$\tan\beta = \sqrt{\frac{\alpha'}{\alpha''}}$$

The Jones matrix is now recast as follows (assuming small absorption[53] $\alpha \ll 1$, $(10^{-\alpha})^{1/2} \approx (1 - \ln(10)\alpha/2) \approx (1 - 1.15\alpha)$, and rotation matrix $\mathbf{R}$ for $\beta \approx 45°$):

$$\mathbf{M}_{Absorption}^{Eigenmodes} = \mathbf{R}^T \mathbf{M}_{Absorption} \mathbf{R} \approx \begin{bmatrix} 1-x & -x \\ -x & 1-x \end{bmatrix},$$

$$x = \ln(10)\alpha/4 \ll 1.$$

The effect of absorption by the dipoles can be described as a projection of the light wave's field vector $\mathbf{E}$ along and normal to the direction of the induced dipole (Fig. 19). The absorption

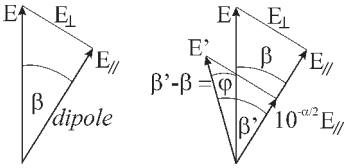

Fig. 19 Model for azimuthal rotation based on absorption of dipoles inclined towards the eigenmodes of the host. It is assumed that the perturbation to the refractivity of the host crystal due to the dye molecules is small.

along the dipole is derived from α' and α'': $\alpha^{\text{dipole}} = \alpha''/\cos^2\beta$. Vector addition of the $\mathbf{E}$ field components along the dipole yields a polarization that appears to be rotated by the angle $\varphi = (\beta' - \beta)$. We call this phenomenon anomalous azimuthal rotation (AAR).

Consistent with experiment, the angle φ changes sign upon flipping the sample 180° around one of the eigenmode directions and upon rotating the sample 90° about the wave vector of the incident light. Abiding by the convention that an optical rotatory effect is considered positive when rotation is clockwise facing the light source (which means that an induced dipole inclined clockwise from the electric field vector of the incoming wave corresponds to a negative or levorotation), we find the following Jones matrix describing AAR as a result of the absorption by the dye measured along the eigenmodes of the host crystal:

$$\mathbf{M}_{AAR} \approx \begin{bmatrix} 1 & \varphi \\ \varphi & 1 \end{bmatrix}, \quad -\varphi = \frac{1.15\alpha''}{1-1.15\alpha''}, \quad \alpha'' \ll 1;\ \beta = 45°,$$

(φ in rad in above equation). This matrix is very similar to that of OR except that in this case the off diagonal elements have the same sign.

4.5.2. Dyed $LiKSO_4$. An effect analogous to AAR can be revealed by the CDIM (now more appropriately called circular extinction imaging microscope, CEIM) that we call anomalous circular extinction (ACE). ACE is strong in $LiKSO_4$ crystals that have oriented and overgrown the dye Chicago sky blue (**4**).[54] Dyed, hexagonal crystals ($P6_3$) are represented in Fig. 20.

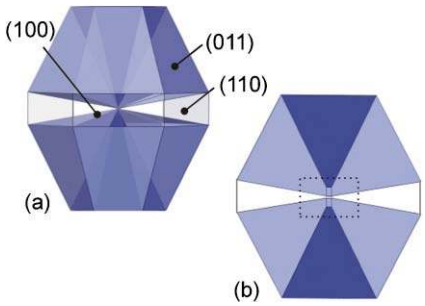

Fig. 20 Idealized representation of a Chicago sky blue (**4**) dyed $LiKSO_4$ crystal. (a) As grown crystal and (b) (100) slice.

The (001) growth sectors were heavily colored whereas the (011) growth sectors were less optically dense by a factor of 4. When viewed through the (100) face with the CEIM described in Section 3.4, the crystals showed a strong differential transmission near the absorption maximum of the dye in the lightly dyed sectors. The micrograph revealed four quadrants with adjacent sectors having opposite sign, a consequence of the well-known enantiomorphous twinning of $LiKSO_4$ previously revealed by X-ray topography (Fig. 21).[55]

In the dyed $LiKSO_4$ sample that we now know to possess LB and ACE, the amplitudes $A'_{\pm}$ are then:

$$A'_{\pm} = \begin{bmatrix} A'_{1\pm} \\ A'_{2\pm} \end{bmatrix} = \mathbf{M}_{AAR,LB} = \begin{pmatrix} e^{ix} & \frac{\varphi}{x}\sin x \\ \frac{\varphi}{x}\sin x & e^{-ix} \end{pmatrix} \frac{1}{\sqrt{2}} \begin{bmatrix} 1 \\ \pm i \end{bmatrix} E_0 =$$

$$\begin{pmatrix} e^{ix} \pm i\frac{\varphi}{x}\sin x \\ \frac{\varphi}{x}\sin x \pm ie^{-ix} \end{pmatrix} \frac{1}{\sqrt{2}} E_0 = \begin{pmatrix} \cos x + i\sin x \pm i\frac{\varphi}{x}\sin x \\ \frac{\varphi}{x}\sin x \pm i\cos(-x) \mp \sin(-x) \end{pmatrix} \cdot$$

$$\frac{1}{\sqrt{2}} E_0$$

The intensities follow from:

$$A'^{*}_{\pm} \cdot A'_{\pm} = \frac{1}{2} E_0^2 (A'^{*}_{1\pm} A'_{1\pm} + A'^{*}_{2\pm} A'_{2\pm}) =$$

$$E_0^2 \{\cos^2 x + (\sin x \pm \frac{\varphi}{x}\sin x)^2\}$$

$$\frac{I'_{\pm}}{E_0^2} = 1 \pm 2\varphi\frac{\sin^2 x}{x} + \varphi^2\frac{\sin^2 x}{x^2}$$

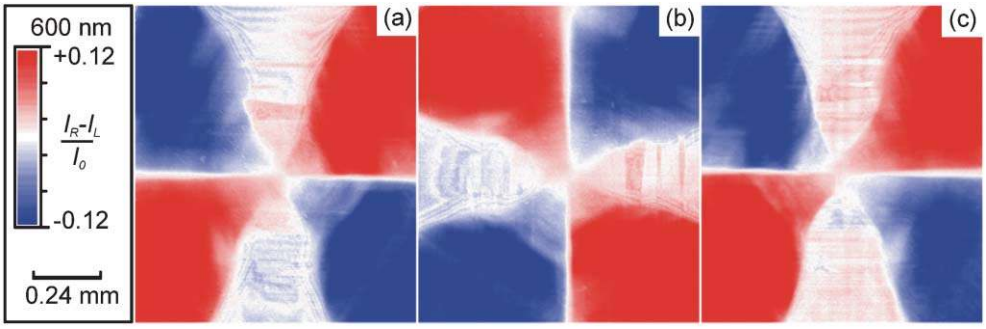

Fig. 21 Circular extinction micrographs of $LiKSO_4$ dyed with **4** resulting from anomalous circular extinction. (a) Center of crystal, (b) Crystal rotated by 90°, (c) Crystal flipped around a vertical axis. Here, one can see that the ACE is invariant with respect to rotation but anti-symmetric with respect to the direction of the wave vector.

and we find indeed a difference in light intensities for the transmission of left and right circularly polarized light:

$$\frac{I'_R - I'_L}{I_0} = 4\varphi \frac{\sin^2(\delta/2)}{\delta/2}$$

Thus, differential circular extinction contrast can result, but only if the sample is birefringent and the phase $\delta \neq n2\pi$, where $n = 1, 2, 3\ldots$.

5. Outlook

In principle, a single instrument could be constructed to accurately measure and separate the contributions of LB, LD, OR, and CD through modifications of the optical path and mechanically modulated linearly and circularly polarized light input. We aspire to construct such an instrument, the natural culmination of the studies discussed herein.

There are a variety of other physical properties of crystals that have been reduced to images *via* novel microscopies. The work of Hulliger and coworkers in the development of scanning pyroelectric microscopy and phase sensitive second harmonic generation is particularly imaginative.[56] While these techniques do not necessarily fall within the theme that we have emphasized in this review – the unfolding of convolved optical properties through the analysis of intensity measurements in polarized light – these other techniques are complementary in the insights that they yield and might certainly lead to a much deeper understanding of the materials that we have discussed here.

Acknowledgements

This work was supported by the USA National Science Foundation (BK), the Petroleum Research Fund of the American Chemical Society (BK, WK), and the University of Washington Royalty Research Fund (WK). KC received fellowship support from the American Chemical Society and the International Centre for Diffraction Data. We are most grateful for the contributions of the individual researchers acknowledged in the studies cited, especially Guy Crundwell for preparing the halite thin sections, Loyd Bastin and Morten Andreas Geday for growing K_2SO_4, and Alex Sodt for preliminary studies of the chiroptical properties of the mixed halates.

References

1 N. H. Hartshorne and A. Stuart, *Crystals and the Polarizing Microscope*, 4th edn., Edward Arnold, London, 1970; A. V. Shubnikov, *Principles of Optical Crystallography*, Consultants Bureau, New York, 1960.
2 W. Kaminsky, *Rep. Prog. Phys.*, 2000, **63**, 1575–1640.
3 W. Mickols, I. Tinoco, Jr., J. E. Katz, M. F. Maestre and C. Bustamante, *Rev. Sci. Instrum.*, 1985, **56**, 2228–2236.
4 W. Mickols, M. F. Maestre, I. Tinoco, Jr. and S. H. Embury, *Proc. Natl. Acad. Sci. USA*, 1985, **82**, 6527–6531; W. E. Mickols, J. D. Corbett, M. F. Maestre, I. Tinoco, Jr., J. Kropp and S. H. Embury, *J. Biol. Chem.*, 1988, **263**, 4338–4346.
5 Maestre, Tinoco, and Bustamante further recognized that when examining anisotropic, chiral, biological structures, the difference in Rayleigh scattering between distinct polarization states contributed to their differential polarization images. This was of particular concern, and benefit, with circularly polarized illumination. Since CD usually involves the measurement of smaller differences than LD the difference in the transmission of left and right circularly polarized light can be dominated by Rayleigh scattering, a phenomenon called circular intensity differential scattering, CIDS. I. Tinoco, Jr., W. Mickols, M. F. Maestre and C. Bustamante, *Annu. Rev. Biophys. Chem.*, 1987, **16**, 319—349.
6 W. Mickols, M. F. Maestre and I. Tinoco, Jr., *Nature*, 1987, **328**, 452–454.
7 D. A. Beach, C. Bustamante, K. S. Wells and K. M. Foucar, *J. Biophys. Soc.*, 1988, **53**, 449–456; D. A. Beach, K. S. Wells, F. Husher and C. Bustamante, *Rev. Sci. Instrum.*, 1987, **58**, 1987–1995.
8 J. D. Corbett, W. E. Mickols and M. F. Maestre, *J. Biol. Chem.*, 1995, **270**, 2708–2715.
9 M. F. Maestre and J. E. Katz, *Biopolymers*, 1982, **21**, 1899–1908. See alsoM. F. Maestre, G. C. Salzman, R. A. Tobey and C. Bustamante, *Biochemistry*, 1985, **24**, 5152–5157; F. Livolant, W. Mickols and M. F. Maestre, *Biopolymers*, 1988, **27**, 1761; F. Livolant and M. F. Maestre, *Biochemistry*, 1988, **27**, 3056–3068.
10 Y. Shindo, M. Nishio and S. Maeda, *Biopolymers*, 1990, **30**, 405–413; Y. Shindo and Y. Ohmi, *J. Am. Chem. Soc.*, 1985, **107**, 91–97.
11 K. W. Hipps and G. A. Crosby, *J. Phys. Chem.*, 1979, **83**, 555–562.
12 J. Schellman and H. P. Jensen, *Chem. Rev.*, 1987, **87**, 1359–1399.
13 R. L. Disch and D. I. Sverdlik, *Anal. Chem.*, 1969, **41**, 82–86.
14 B. Nordén, *Acta Chem. Scand.*, 1972, **26**, 1763–1776; Å. Davidsson and B. Nordén, *Spectrochim. Acta, Part A*, 1976, **32**, 717–722; Å. Davidsson, B. Nordén and S. Seth, *Chem. Phys. Lett.*, 1980, **70**, 313–316.
15 J. T. Cheng, L. A. Nafie and P. J. Stephens, *J. Opt. Soc. Am.*, 1975, **65**, 1031–1035.
16 M. J. B. Tunis-Schneider and M. F. Maestre, *J. Mol. Biol.*, 1970, **52**, 521–541; C. Nuckolls, T. Katz, T. Verbiest, S. Van Elshocht, H.-G. Kuball, S. Kiesewalter, A. J. Lovinger and A. Persoons, *J. Am. Chem. Soc.*, 1998, **120**, 8656–8660.
17 H.-G. Kuball and J. Altschuh, *Chem. Phys. Lett.*, 1982, **87**, 599–603.
18 R. Kuroda, T. Harada and Y. Shindo, *Rev. Sci. Instrum.*, 2001, **72**, 3802–3810.
19 T. Yamada, H. Onuki, M. Yuri and S. Ishizaka, *Jpn. J. Appl. Phys.*, 2000, **39**, 310–315.
20 G. N. Ramachandran and S. Ramaseshan, *J. Opt. Soc. Am.*, 1952, **42**, 49–56; H. G. Jerrard, *J. Opt. Soc. Am.*, 1954, **44**, 634–640.
21 H. Mueller, *J. Opt. Soc. Am.*, 1948, **38**, 661.
22 R. C. Jones, *J. Opt. Soc. Am.*, 1941, **31**, 488–493.
23 W. A. Shurcliff, *Polarized Light*, Harvard University Press, Cambridge, Mass., 1966.
24 A. M. Glazer, J. G. Lewis and W. Kaminsky, *Proc. R. Soc. London, Ser. A*, 1996, **452**, 2751–2765.
25 R. D. Allen, J. Brault and R. Moore, *J. Cell Biol.*, 1963, **18**,

223–235; D. J. Benard and W. C. Walker, *Rev. Sci. Instrum.*, 1976, **47**, 122–127.
26 J. Kobayashi and Y. Uesu, *J. Appl. Crystallogr.*, 1983, **16**, 204–211; J. Kobayashi, Y. Uesu and H. Takahashi, *J. Appl. Crystallogr.*, 1983, **16**, 212–219.
27 J. Schellman and H. P. Jensen, *Chem. Rev.*, 1987, **87**, 1359–1399.
28 J. O. Stenflo and H. A. Povel, *Appl. Opt.*, 1985, **24**, 3893–3898; H. Povel, *Opt. Eng.*, 1995, **34**, 1870–1878.
29 H. Povel, H. Aebersold and J. O. Stenflo, *Appl. Opt.*, 1990, **29**, 1186–1190.
30 K. Andert, W. Schälike, B. Bölting, R. Pittelkow, R. Wetzel and G. Snatzke, *Rev. Sci. Instrum.*, 1991, **62**, 1912–1915.
31 D. R. Bobbitt, in *Analytical Applications of Circular Dichroism* (N. Purdie; H. G. Brittain, eds.), Elsevier, New York, 1994.
32 J. R. L. Moxon and A. R. Renshaw, *J. Phys.: Condens. Matter*, 1990, **2**, 6807–6836; M. Kremers and H. Meekes, *J. Phys. D: Appl. Phys.*, 1995, **28**, 1212–1224.
33 A. Authier, ed., *International Tables for Crystallography, Volume D: Physical Properties of Crystals*, Kluwer, Dordrecht, 2003.
34 G. O. Jones, J. Kreisel, V. Jennings, M. A. Geday, P. A. Thomas and A. M. Glazer, *Ferroelectrics*, 2002, **270**, 1377–1382; M. Geday, J. Kreisel, A. M. Glazer and K. Roleder, *J. Appl. Crystallogr.*, 2000, **33**, 909–914.
35 D. Zekria and A. M. Glazer, *J. Appl. Crystallogr.*, 2004, **7**, 143–149.
36 C. Hernandez-Rodriguez, M. A. Geday, J. Kreisel, A. M. Glazer and A. Hidalgo-Lopez, *J. Appl. Crystallogr.*, 2003, **36**, 914–919.
37 M. D. Hollingsworth and M. L. Peterson, *Proc. NASA Microgravity Materials Science Conference, 2002*, NASA, Washington, DC; D. Gillies, N. Ramachandran, K. Murphy, P. McCauley and N. Bennett, eds., pp. 283–288, Feb. 2003.
38 M. Vaida, L. J. W. Shimon, Y. Weisinger-Lewin, F. Frolow, M. Lahav, L. Leiserowitz and R. K. McMullan, *Science (Washington)*, 1988, **241**, 1475–1479; J. M. McBride and S. B. Bertman, *Angew. Chem., Int. Ed. Engl.*, 1989, **28**, 330–333.
39 P. Gopalan, M. L. Peterson, G. Crundwell and B. Kahr, *J. Am. Chem. Soc.*, 1993, **115**, 3366–3367; P. Gopalan, G. Crundwell, A. Bakulin, M. L. Peterson and B. Kahr, *Acta Crystallogr., Sect. B*, 1997, **53**, 189–202.
40 B. Kahr and J. M. McBride, *Angew. Chem., Int. Ed. Engl.*, 1992, **31**, 1–32; R. Brauns, *Die optischen Anomalien in der Krystalle*, S. Hirzel, Leipzig, 1891.
41 W. Kaminsky, *WinXMorph*, 2004.
42 M. Geday and A. M. Glazer, *J. Appl. Crystallogr.*, 2002, **35**, 185–190.
43 G. N. Ramachandran and S. Ramaseshan, *Handbuch der Physik*, Vol. XXV/1, Springer-Verlag, Berlin, 1961, pp. 1–217.
44 B. Kahr and R. W. Gurney, *Chem. Rev.*, 2001, **101**, 893–951.
45 L. D. Bastin and B. Kahr, *Tetrahedron*, 2000, **56**, 6633–6643.
46 W. Kaminsky, *Phase Transitions*, 1996, **59**, 121–133.
47 W. Kaminsky, *Ferroelectrics*, 1997, **204**, 233–246.
48 W. Kaminsky and A. M. Glazer, *Phase Transitions*, 1998, **66**, 1–21.
49 H. Marbach, *Ann. Phys. Chem.*, 1856, **9**, 459; H. Marbach, *Ann. Phys. Chem.*, 1858, **99**, 451.
50 J. M. Bijvoet, *Acta Crystallogr.*, 1960, **13**, 1100–1101.
51 S. Chandrasekhar and M. S. Madhava, *Mater. Res. Bull.*, 1969, **4**, 489–494; T. Niedermaier and W. Schlenk, Jr., *Chem. Ber.*, 1972, **105**, 3470–3478; V. Sivaramakrishnan and K. A. Arunkumar, *Opt. Acta*, 1976, **23**, 209–216.
52 P. Gopalan, M. L. Peterson, G. Crundwell and B. Kahr, *J. Am. Chem. Soc.*, 1993, **115**, 3366–3367; P. Gopalan, G. Crundwell, A. Bakulin, M. L. Peterson and B. Kahr, *Acta Crystallogr., Sect. B*, 1997, **53**, 189–202.
53 If the angle β differs from 45°, we can split the Jones matrices into two with one describing LD oriented along the eigen modes and one describing LD inclined at 45° to the eigen mode directions.
54 K. Claborn, A.-S. Chu, J. Herreros-Cedrés, W. Kaminsky, B. Kahr, submitted.
55 H. Klapper, Th. Hahn and S. Chung, *Acta Crystallogr., Sect. B*, 1987, **43**, 147–159.
56 A. Quintel, J. Hulliger and M. Wübbenhorst, *J. Phys. Chem. B*, 1998, **102**, 4277–4283; J. Hulliger, *Chimia*, 2001, **55**, 1025–1028; S. Kluge, F. Budde, I. Dohnke, P. Rechsteiner and J. Hulliger, *Appl. Phys. Lett.*, 2002, **81**, 247–249; P. Rechsteiner, J. Hulliger and M. Flörsheimer, *Chem. Mater.*, 2000, **12**, 3296–3300; A. Quintel, S. W. Roth, J. Hulliger and M. Wübbenhorst, *Mol. Cryst. Liq. Cryst.*, 2000, **338**, 243–250.